ACS APPLIED MATERIALS & INTERFACES

Research Article

www.acsami.org

Synthesis of Carbon Nanotube–Anatase TiO_2 Sub-micrometer-sized Sphere Composite Photocatalyst for Synergistic Degradation of Gaseous Styrene

Taicheng An,*[,†] Jiangyao Chen,[†,§] Xin Nie,[†,§] Guiying Li,[†] Haimin Zhang,[‡] Xiaolu Liu,[†,‡] and Huijun Zhao*[,‡]

[†]State Key Laboratory of Organic Geochemistry, Guangdong Key Laboratory of Environmental Resources Utilization and Protection, Guangzhou Institute of Geochemistry, Chinese Academy of Sciences, Guangzhou 510640, China

[‡]Centre for Clean Environment and Energy, Griffith University, Gold Coast Campus, QLD 4222, Australia

[§]University of Chinese Academy of Sciences, Beijing 100049, China

Supporting Information

ABSTRACT: The carbon nanotube (CNT)–sub-micrometer-sized anatase TiO_2 sphere composite photocatalysts were synthesized by a facile one-step hydrothermal method using titanium tetrafluoride as titanium source and CNTs as structure regulator. Various technologies including X-ray diffraction, UV–visible absorption spectra, N_2 adsorption–desorption, scanning electron microscopy, and transmission electron microscopy were employed to characterize the structure properties of the prepared composite photocatalysts. The results indicated that the composite photocatalysts consisted of CNTs wrapping around the sub-micrometer-sized anatase TiO_2 spheres with controllable crystal facets and that the aggregated particles with average diameter ranged from 200 to 600 nm. The fabricated composite photocatalysts were used to degrade gaseous styrene in this work. As expected, a synergistic effect that remarkably enhancing the photocatalytic degradation efficiency of gaseous styrene by the prepared composite photocatalysts was observed in comparison with that the degradation efficiency using pure anatase TiO_2 and the adsorption of CNTs. Similar results were also confirmed in the decolorization of liquid methyl orange. Further investigation demonstrated that the synergistic effect in the photocatalytic activity was related to the structure of the sub-micrometer-sized anatase TiO_2 spheres and the significant roles of CNTs in the composite photocatalysts. By controlling the content of CNTs, the content of TiO_2 or the temperature during the hydrothermal synthesis process, anatase TiO_2 spheres with controllable crystallite size and dominant crystal facets such as {001}, {101}, or polycrystalline could be obtained, which was beneficial for the increase in the synergistic effect and further enhancement of the photocatalytic efficiencies.

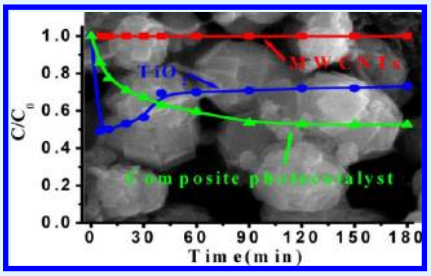

KEYWORDS: *CNT-based composite photocatalyst, TiO_2 spheres, structure regulation, photocatalytic activity, synergistic effect*

1. INTRODUCTION

Styrene, as a derivative of benzene and one of important volatile organic compounds (VOCs), is a colorless oily liquid that evaporates easily and has an unpleasant odor at high concentrations. Continuous exposure to small quantities of styrene has shown to cause neurotoxic, hematological, cytogenetic and carcinogenic effects in humans.[1,2] Thus, the threshold limit value recommended by the American Conference of Governmental Industrial Hygienists is only 20 ppm.[3] Most styrene is from anthropogenic emission because it is a commercially important chemical widely used in the manufacture of synthetic rubber, resins, polyesters and plastics.[4] Therefore, the removal of VOCs such as gaseous styrene is of important for environmental protection.

Different kinds of physical, chemical, and biological techniques have been utilized to remove VOCs from air.[5−8] Among different end-of-pipe abatement techniques, activated carbon adsorption is the most widely used. However, such techniques are capable only of converting the gaseous form of organic pollutants into the adsorbed forms while the absolute toxicity of the substances still remains.[9] In recent years, heterogeneous photocatalytic technology has attracted increasing attention because of the fact that it is a green technology that can be widely applied to environmental remediation.[10−13] To date, various photocatalysts such as metal oxides and chalcogenides have been developed for VOCs abatement.[14−20] In this regard, TiO_2 has been the dominant photocatalyst because of its superior photocatalytic oxidation ability, high photocorrosion resistance, and nontoxic and inexpensive characteristics.[11,21−24] Unfortunately, the concentration of pollutants in air environment is quite low and the adsorption of gaseous pollutants onto the TiO_2 photocatalyst is often

Received: August 13, 2012
Accepted: November 6, 2012
Published: November 6, 2012

limited because of its small specific surface area, leading to very low photocatalytic degradation efficiency. A possible way to overcome this is to add a coadsorbent to the TiO_2 photocatalyst to enhance the total removal efficiency of pollutants.[25−27]

Carbon nanotubes (CNTs) recently attracted considerable interest since being discovered in 1991 by Iijima[28,29] because of their unusual mechanical, electrical, and chemical properties. Because of its hollow and layered structures with large specific surface area, CNTs is very suitable for the enrichment of low-concentration VOCs, which makes it a promising coadsorbent or support for gas−solid phase catalysis. A significant interest has therefore been dedicated to enhance the photocatalytic activity of TiO_2 to VOCs by using CNTs.[30−33] In these reports, the enhanced of photocatalytic activity for a TiO_2/CNT composite has been attributed to the effect of CNTs as an electron reservoir to suppress the charge recombination. However, the photocatalytic degradation performance of TiO_2/CNT composites could also be strongly affected the particle size, crystalline phase, crystallinity, surface area and crystal facets of TiO_2.[34−40] Hence, it should be a topic of interest to utilize the special effect of CNTs to obtain the desired TiO_2 structure with high photocatalytic activity. Xu et al.[31] and Bouazza et al.[32] proposed that CNTs could act as a dispersing template or support to control the TiO_2 morphology, affecting the photocatalytic activity. However, it is still a challengeable task to fully understand the relationship between the photocatalytic activity and the structure characteristic of CNTs based composite photocatalyst, as well as the synergistic effect in the photocatalytic degradation of organic pollutants in aqueous and gas phase.

Herein, a series of composite photocatalysts of carbon nanotube−sub-micrometer-sized anatase TiO_2 spheres have been successfully synthesized by a facile one-step hydrothermal route using titanium tetrafluoride (TiF_4) as titanium source and CNTs as structure regulator. The effect of important parameters (i.e., the amount of CNTs, the amount of TiF_4, hydrothermal reaction temperature and time) on the structural properties of the resultant photocatalyst was been systematically investigated. Importantly, the relationships between the photocatalytic activities and the structural characteristics of the composite photocatalysts was investigated and discussed in detail using degradation of gaseous phase styrene and methyl orange (MO) in aqueous phase as model pollutants.

2. EXPERIMENTAL SECTION

2.1. Synthesis of Photocatalysts. Two grams of multiwall carbon nanotubes (MWCNTs), purchased from Shenzhen Nanotech Port Co., Ltd., China with the diameter of 60−100 nm and length of 5−15 μm, were first purified by refluxing in 80 mL mixture of concentrated sulphuric acid (95%-98%) and nitric acid (65%-68%) with a volume ratio of 3:1 under the temperature of 90 °C for 90 min, in order to remove the amorphous carbon, metal catalyst, and introduce oxygenated functionalities on the nanotube surface.[41] Then dry MWCNTs were obtained by the sequence process of filtering, washing with distilled water, and drying at 80 °C.

For the synthesis of MWCNT−TiO_2 sphere composite photocatalysts, a given amount of purified MWCNTs was first dispersed in 40 mL of TiF_4 (Acros Organics, 99%) aqueous solution with different concentrations. After being ultrasonicated for 30 min, the mixtures were transformed into 100 mL Teflon-line autoclaves and kept at selected temperatures and at different intervals in an oven. After hydrothermal reaction, the products were collected by centrifuge, washed with distilled water thoroughly, and finally dried at 80 °C for 8 h. The experimental details are given in the Supporting Information.

2.2. Characterization of Structure and Morphology. The synthesized photocatalysts were comprehensively characterized by X-ray diffractometer (XRD, Rigaku Dmax X-ray diffractometer), UV−visible spectrophotometer (UV−vis, UV-2501PC), nitrogen adsorption apparatus (Micromeritics ASAP 2020 system), scanning electron microscopy (SEM, JSM-6330F), and transmission electron microscopy (TEM, JEM-2010).

2.3. Characterization of Adsorption Ability and Photocatalytic Activity. Figure S1a (Supporting Information) shows the schematic diagram of the experimental setup for the adsorption and photocatalytic degradation of gaseous styrene. Gaseous styrene with the concentration of 25 ± 1.5 ppmv was stably and continuously fed into a cubic quartz glass reactor, with the size of 1.0 cm × 1.0 cm × 0.5 cm (see Figure S1b in the Supporting Information) where 0.10 g of prepared photocatalysts was loaded, with dry air at a total flow rate of 20 mL/min. A 365 nm UV-LED spot lamp (Shenzhen Lamplic Science Co., Ltd.) was used as a light source which was fixed vertically top of the reactor with the distance of 6 cm (the UV intensity was controlled at 70 mW/cm^2). Before the lamp was switched on, the pollutant was allowed to reach the gas−solid adsorption equilibrium. The concentrations of pollutant were analyzed by a gas chromatography (GC-900A) equipped with a flame ionization detector. The temperatures of the column, injector, and detector were 110, 230, and 230 °C, respectively. Gas samples were collected at regular intervals using a gastight locking syringe (Agilent, Australia), and a 200 μL gas sample was injected into the column for concentration determination in the splitless mode.

Figure S2 (Supporting Information) shows the schematic diagram of the experimental setup for photocatalytic decolorization of liquid phase MO. Initially, 10 mg of prepared photocatalysts was initially added into 90 mL of distilled water. The mixture was ultrasonicated for 1 min to ensure good dispersion of the powder, followed by adding 10 mL of MO solution with the concentration of 100 mg/L. Before switching the 125 W high-pressure mercury lamp with a maximum emitting radiation of 365 nm (GGZ125, Shanghai Yaming Lighting Co., Ltd., the UV intensity was controlled at 1.17 mW/cm^2), 30 min dark adsorption was allowed in a quartz tube reactor with a jacket outside to ensure the establishment of adsorption−desorption equilibrium. A 3 mL solution, taken at a given time intervals and filtered through a 0.22 μm Millipore filter, was used to analyze the concentration of MO on an UV−vis spectrophotometer (756PC) at a wavelength of 464 nm.

The photocatalytic degradation and decolorization efficiency were calculated according to the eq 1 and 2 for styrene and MO, respectively

$$\text{degradation efficiency} = C/C_0 \quad (1)$$

$$\text{decolorization efficiency} = C/C_0 \quad (2)$$

where C presented the content of residual pollutant and C_0 was its original content.

3. RESULTS AND DISCUSSION

3.1. XRD Analysis. The wide-angle XRD patterns of all prepared samples are displayed in Figure 1. The characteristic diffraction peaks of the XRD patterns for all samples at 2θ = 25.3, 37.8, 48.0, 54.0, 55.3, 62.4, and 68.7° are attributed to the {101}, {004}, {200}, {105}, {211}, {204}, and {112} planes of anatase TiO_2.

The XRD patterns shown in Figure 1a revealed no obvious diffraction peaks of MWCNTs at 2θ = 26.0° for samples containing 7.2, 18.9, and 31.7 wt % MWCNTs, possibly because the main peak at 2θ = 26.0° was covered by the main peak of anatase TiO_2 at 2θ = 25.3°.[42] When the content of MWCNTs increased to 48.2 wt %, an obvious characteristic peak at 2θ = 26.0° could be observed. Table 1 summarizes the crystallite sizes of TiO_2 particles for all samples estimated by XRD from the TiO_2 peak at 2θ = 48.0°, where there was

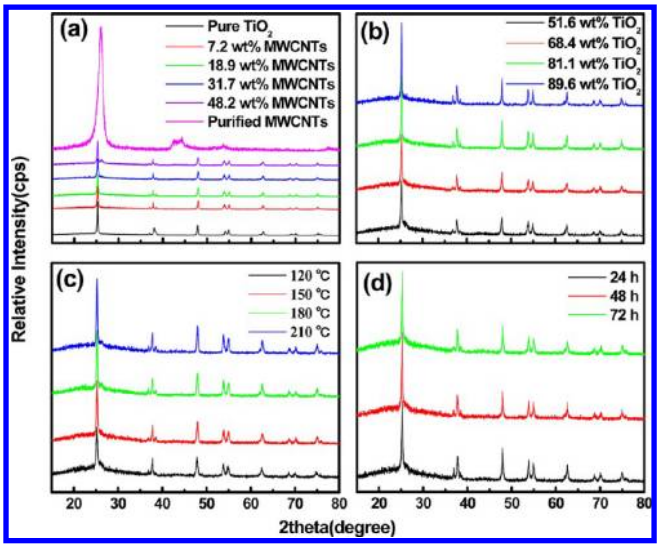

Figure 1. XRD patterns of (a) purified MWCNTs, prepared pure TiO_2, and composite photocatalysts prepared with different MWCNTs contents. (TiO_2 content, from 92.8 to 51.8 wt %; hydrothermal temperature, 150 °C; hydrothermal time, 72 h); (b) composite photocatalysts prepared with different TiO_2 contents (MWCNT content, from 48.4 to 10.4 wt %); hydrothermal temperature: 150 °C; hydrothermal time: 72 h); (c) composite photocatalysts prepared under different hydrothermal temperatures (MWCNT content, 31.6 wt %; TiO_2 content, 68.4 wt %; hydrothermal time, 72 h); (d) composite photocatalysts prepared with different hydrothermal times (MWCNT content, 31.6 wt %; TiO_2 content, 68.4 wt %; hydrothermal temperature, 150 °C).

Table 1. Crystallite Size of TiO_2 in Pure TiO_2 and MWCNT-TiO_2 Sphere Composite Photocatalysts

samples prepared under different conditions	crystallite size (nm)
pure TiO_2	44.7
7.2 wt % MWCNTs	33.1
18.9 wt % MWCNTs	30.1
31.7 wt % MWCNTs	29.9
48.2 wt % MWCNTs	30.6
51.6 wt % TiO_2	23.2
68.4 wt % TiO_2	26.7
81.1 wt % TiO_2	30.1
89.6 wt % TiO_2	35.2
120 °C	24.2
150 °C	26.7
180 °C	27.3
210 °C	28.4
24 h	25.5
48 h	26.5
72 h	26.7

ignorable interference from MWCNTs.[30,43] It could be seen from Table 1 that the average crystallite size of pure TiO_2 particles was ca. 44.7 nm, and those decreased from 33.1 to 29.9 nm with increased MWCNTs content from 7.2 to 31.7 wt %, suggesting that the presence of MWCNTs hindered the growth of the TiO_2 particles.[30] However, a further increase in the MWCNTs to 48.2 wt % showed a slight increased crystallite size to 30.6 nm, due to the rapid hydrolysis of the titanium precursor.[43] Deduced from the XRD patterns shown in Figure 1b, it was found that an increase in the TiO_2 content results in an increase in the intensity of diffraction peak at 2θ = 48.0° and a decrease in the peak width, implying an increased in the crystallite size. As shown in Table 1, the TiO_2 crystallite size was increased from 23.2 to 35.2 nm when the TiO_2 content was increased from 51.6 to 89.6 wt %.

Figures 1c and d show the XRD patterns of the samples prepared with different hydrothermal temperature and time, respectively. As expected, an increase in the hydrothermal reaction temperature or time resulted in an increase in the crystallinity. The TiO_2 crystallite size increased from 24.2 to 28.4 nm with the hydrothermal temperature increased from 120 to 210 °C, while an increase in the reaction time from 24 to 72 h resulted in a slight increase in the crystallite size from 25.5 to 26.7 nm.

3.2. UV–Vis Analysis. The UV–vis absorption spectra of P25, the as-prepared pure TiO_2, purified MWCNTs and the as-prepared MWCNTs – sub-micrometer-sized anatase TiO_2 sphere composite photocatalysts with different MWCNTs contents were obtained (see Figure S3 in the Supporting Information). An increased visible-light absorption for the MWCNTs-TiO_2 sphere composite photocatalysts was observed as the MWCNTs content was increased.[30] All samples exhibited the typical absorption with an intense transition in the UV region of the spectra except the purified MWCNTs attributing to the electron transition of TiO_2 from the valence band to conduction band.[10,31,44] Further investigation indicated that no obvious variation for the absorption intensity in UV region was observed for the composite photocatalysts with different MWCNTs contents. This might be because that the MWCNTs were mostly covered by the TiO_2 spheres. By comparing the absorption intensity of MWCNTs-TiO_2 sphere composite photocatalysts and P25 in the UV region, it was found that the MWCNTs-TiO_2 sphere composite photocatalysts presented more intense absorption than that of P25 at the wavelength of 365 nm (which is the single wavelength of UV-LED lamp used in the photocatalytic experiments of gaseous styrene), although P25 showed stronger absorption intensity in the wavelength region of 250–320 nm.

3.3. N_2 Adsorption–Desorption Analysis. Nitrogen adsorption and desorption isotherms as well as pore diameter distribution of the as-prepared pure TiO_2, purified MWCNTs and the as-prepared MWCNTs –TiO_2 sphere composite photocatalysts with different MWCNTs contents are shown in Figure 2. It can be seen that all isotherms were of type IV (IUPAC classification) with a typical H3 hysteresis loop, indicating the existence of mesoporous structure and slit-like pores.[45] The average pore sizes of the pure TiO_2, purified MWCNTs, as well as composite samples with 7.2, 18.9, 31.7, and 48.2 wt % MWCNTs were very similar with pore sizes of 3.29, 3.74, 3.67, 3.78, 3.71, and 3.82 nm, respectively (the inset of Figure 2). The quantitative details about the Brunauer–Emmett–Teller (BET) surface areas, Barrett–Joyner–Halen (BJH) total pore volumes and average pore diameter were listed in Table 2. Purified MWCNTs had the largest surface area (59.22 m^2/g) and total pore volume (0.245 cm^3/g), whereas pure TiO_2 showed the smallest BET surface area (6.34 m^2/g) and total pore volume (0.020 cm^3/g). As for composite samples, with increased MWCNTs content from 7.2 to 48.2 wt %, both the BET surface area and the total pore volume were increased from 21.13 to 55.20 m^2/g and from 0.045 to 0.215 cm^3/g, respectively. Larger BET surface area and bigger total pore volume might lead to higher adsorption capacity toward pollutants, which could be verified by the results displayed in the followed adsorption experiments.

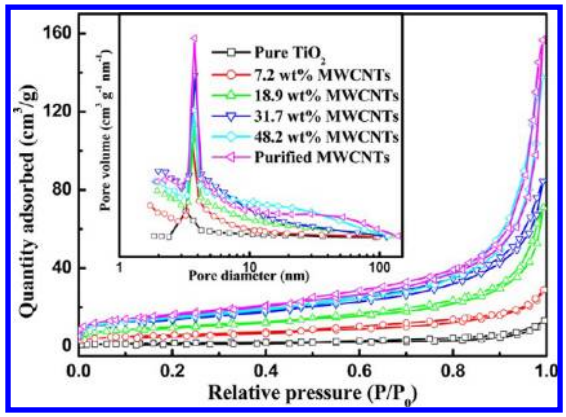

Figure 2. N_2 adsorption−desorption isotherm and pore-size distribution curves of pure TiO_2, purified MWCNTs and composite photocatalysts prepared with different contents of MWCNTs (TiO_2 contents, from 92.8 to 51.8 wt %; hydrothermal temperature, 150 °C; hydrothermal time, 72 h).

Table 2. Structure Parameters of Pure TiO_2, Purified MWCNTs, and Composite Photocatalysts

samples	BET surface area (m^2/g)	avg pore size (nm)	BJH total pore volume (cm^3/g)
pure TiO_2	6.34	3.29	0.02
7.2 wt % MWCNTs	21.13	3.67	0.05
18.9 wt % MWCNTs	35.71	3.78	0.11
31.7 wt % MWCNTs	52.12	3.71	0.13
48.2 wt % MWCNTs	55.20	3.82	0.22
purified MWCNTs	59.22	3.74	0.25

3.4. SEM and TEM Analysis. To thoroughly study the microstructures of the photocatalysts synthesized, the SEM and TEM images of the MWCNTs-TiO_2 sphere composite photocatalysts with different MWCNTs contents were observed (Figure 3). It can be seen that the TiO_2 spheres were well wrapped around by the MWCNTs. Comparing the SEM image of purified MWCNTs and the SEM image of MWCNTs in MWCNTs-TiO_2 composite suggests no noticeable CNT structural changes before and after the hydrothermal synthesis. Further observation indicated that with increased MWCNTs content, more MWCNTs were discerned and the size of the TiO_2 spheres became smaller, confirming the inhibition role of MWCNTs for the growth of TiO_2 particles. For the composite photocatalyst with 7.2 wt % MWCNTs (Figure 3a), the average diameter of TiO_2 spheres was ~600 nm and the surface of the TiO_2 spheres was covered by square-shaped crystalline facets. The TEM image of an individual sphere of this sample is shown in Figure 3b. The corresponding selected-area electron diffraction (SAED) pattern recorded from the red circled area (top inset in Figure 3b) confirmed that the square-shaped crystalline was single crystal with exposed (001) surface.[39] The high-resolution TEM (HRTEM) image (bottom inset in Figure 3b) showed that the lattice fringes spacing of 0.235 nm parallel to the top and bottom facets were assigned to (001) planes of anatase TiO_2.[46] That is, the composite photocatalysts prepared with 7.2 wt % MWCNTs consisted of MWCNTs wrapping around the

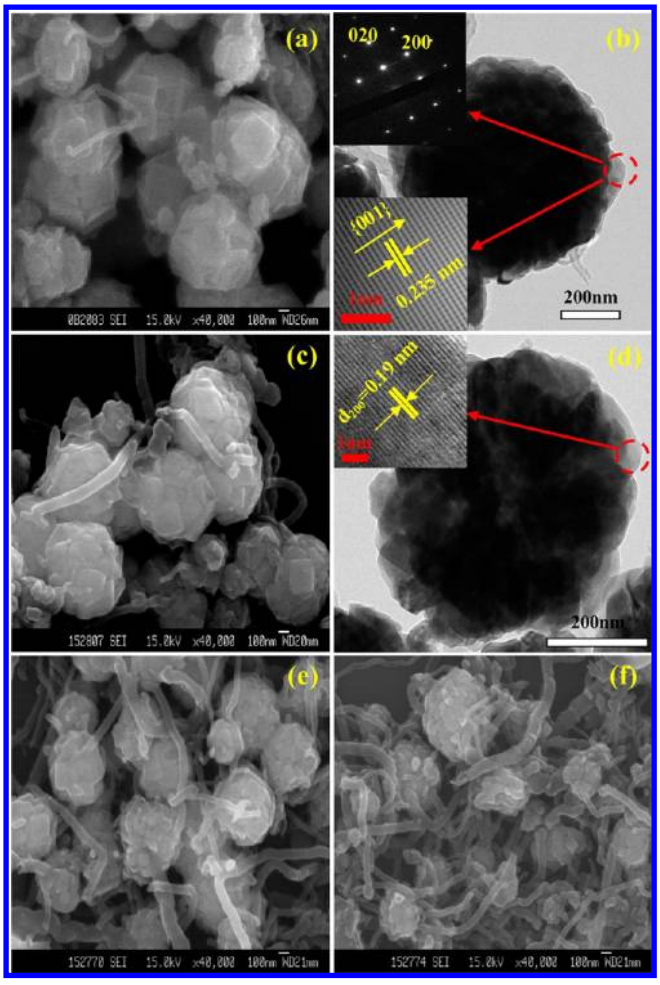

Figure 3. SEM and TEM images of composite photocatalysts prepared with different MWCNTs contents. ((a, b) 7.2 wt %; (c, d) 18.9 wt %; (e) 31.7 wt %; (f) 48.2 wt %; TiO_2 contents, from 92.8 to 51.8 wt %; hydrothermal temperature, 150 °C; hydrothermal time, 72 h).

anatase TiO_2 spheres with exposed single-crystal {001} facets. The percentage of exposed {001} facets was estimated as 74%.

With MWCNTs was increased from 7.2 to 18.9 wt %, the TiO_2 spheres became smaller with the average diameter of ~500 nm and the square-shaped particles on the spheres were melted together (Figures 3c and d). The HRTEM image recorded from the red circled area (inset in Figure 3d) clearly showed the continuous {200} atomic planes with a lattice spacing of 0.19 nm, corresponding to the {200} planes of anatase TiO_2 single crystal.[47] Thus, the dominant facet of single crystals on TiO_2 spheres for composite photocatalyst with the 18.9 wt % MWCNTs was {001} facets and the corresponding percentage of exposed {001} facets decreased to ca. 55%. Further increasing MWCNTs content to 31.7 wt % (Figure 3e), the average diameter of TiO_2 spheres further decreased to ~400 nm and less square-shaped exposed surface could be observed. The percentage of exposed {001} facets continuously decreased to 30%. However, when the MWCNT content reached 48.2 wt % (Figure 3f), TiO_2 spheres became irregular-shaped particles, further confirming that MWCNTs could inhibit the growth of TiO_2 spheres. Under such conditions, a meaningful calculation of the percentage of exposed {001} facets became difficult.

dx.doi.org/10.1021/am3016476 | ACS Appl. Mater. Interfaces 2012, 4, 5988−5996

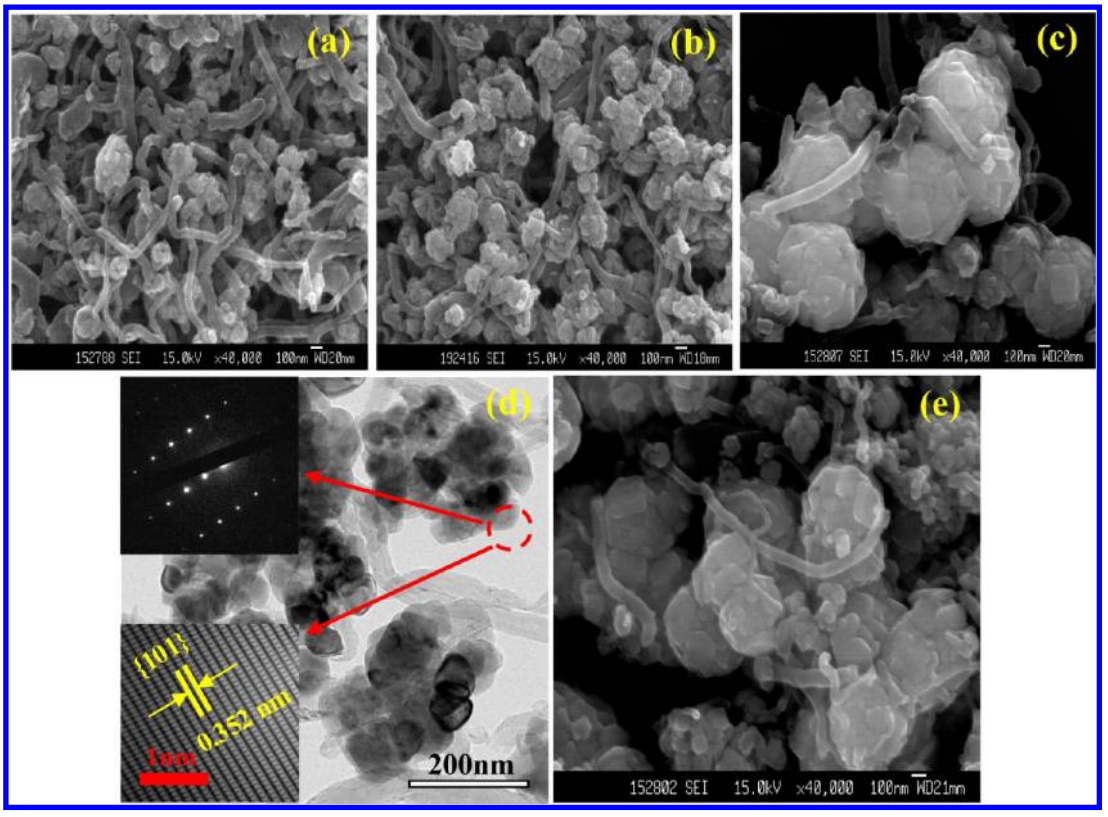

Figure 4. SEM and TEM images of composite photocatalysts prepared with different contents of TiF_4. ((a) 51.6 wt %; (b, d) 68.4 wt %; (c) 81.1 wt %; (e) 89.6 wt %; MWCNT contents, from 48.4 to 10.4 wt %; hydrothermal temperature, 150 °C; hydrothermal time, 72 h).

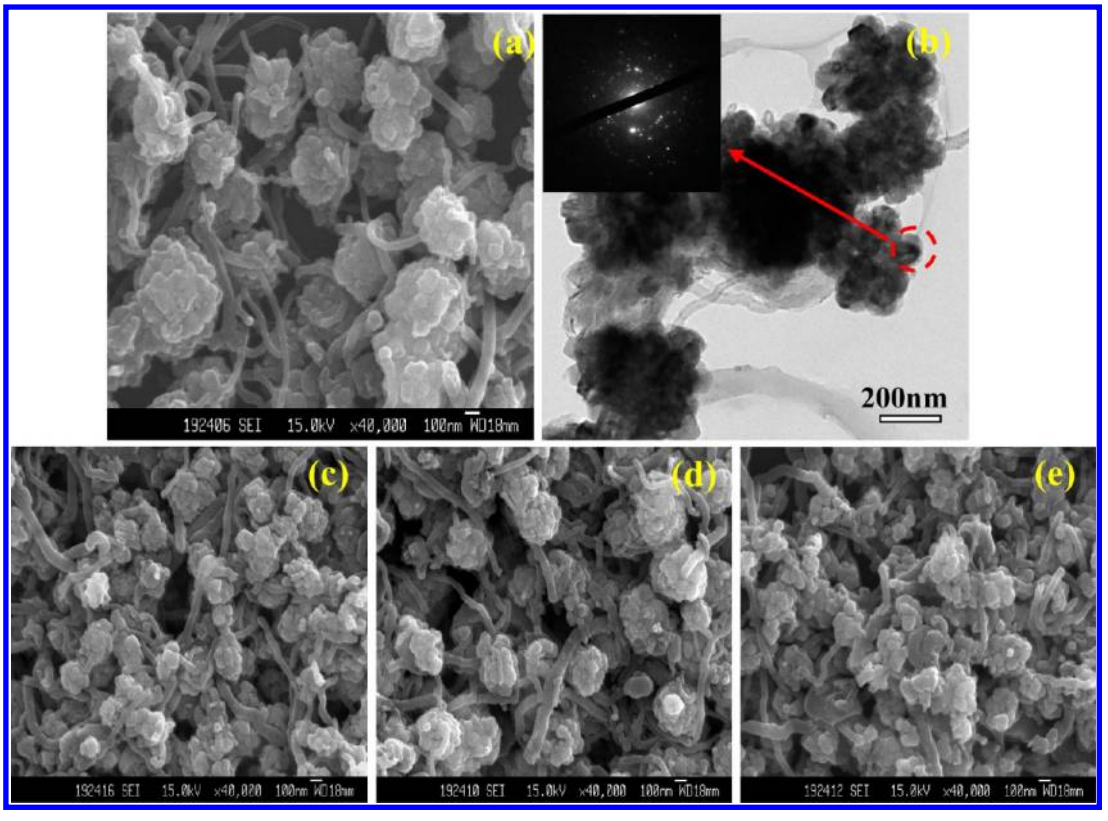

Figure 5. SEM and TEM images of composite photocatalysts prepared under different hydrothermal temperatures. ((a, b) 120 °C; (c) 150 °C; (d) 180 °C; (e) 210 °C; MWCNT content, 31.6 wt %; TiO_2 content, 68.4 wt %; hydrothermal time, 72 h).

dx.doi.org/10.1021/am3016476 | ACS Appl. Mater. Interfaces 2012, 4, 5988−5996

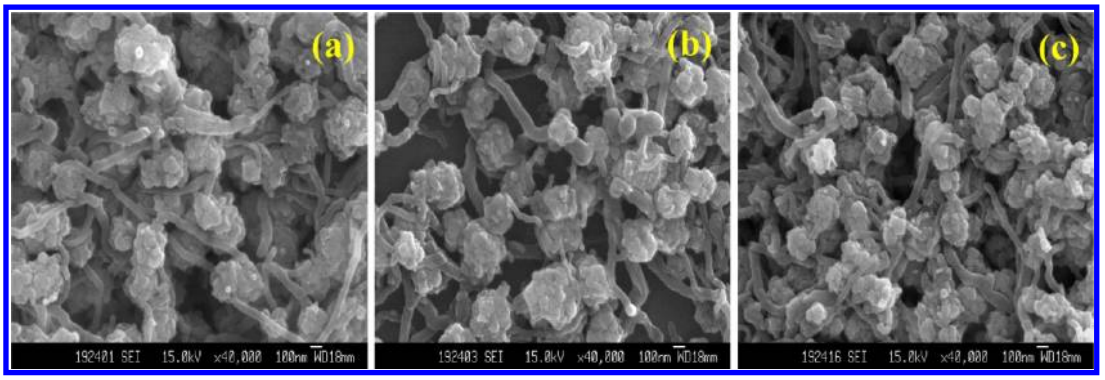

Figure 6. SEM images of composite photocatalysts prepared with different hydrothermal times. ((a) 24 h; (b) 48 h; (c) 72 h; MWCNT content, 31.6 wt %; TiO_2 content, 68.4 wt %; hydrothermal temperature, 150 °C).

Figure 4 shows the effect of the TiO_2 content on the morphology of the as-prepared composite photocatalysts. Obviously, fewer MWCNTs could be observed from the SEM images with the increased TiO_2 content. With 51.6 wt % (Figure 4a) and 68.4 wt % (Figure 4b) of TiO_2, the average diameter of TiO_2 spheres in the samples was ~200 nm. With a further increase in the TiO_2 content from 81.1 (Figure 4c) to 89.6 wt % (Figure 4e), the TiO_2 particles agglomerated and TiO_2 spheres with the average diameter larger than 500 nm were obtained. For the composite photocatalysts with 68.4 wt % TiO_2, the SAED pattern recorded from the red circled area (top inset in Figure 4d) confirmed a good single anatase crystal structure of TiO_2 spheres. The HRTEM image (bottom inset in Figure 4d) revealed a 0.352 nm distance between lattice planes, corresponding to the {101} lattice planes of anatase TiO_2.[48] This result indicated that MWCNTs-TiO_2 sphere composite photocatalyst with 68.4 wt % composed of MWCNTs and TiO_2 spheres with exposed {101} facets. By comparing the SEM and TEM images shown in Figures 3d and 4b–d, it was found that the morphology of particles on the TiO_2 spheres were converted from square shape to irregular shape and the dominant crystal facet was accordingly transformed from {001} facet to {101} facet when TiO_2 content was decreased from 81.1 to 68.4 wt %, suggesting that the morphology and the dominant facet of anatase TiO_2 particles could be controlled by changing the TiO_2 content.

The effect of hydrothermal reaction temperature on the resultant MWCNTs-TiO_2 sphere composites was also investigated and the corresponding SEM and TEM results are shown in Figure 5. The SEM images revealed that with 150 °C, the resultant composite consisted of MWCNTs with TiO_2 spheres having an average diameter of ~200 nm. When the reaction temperature was increased from 150 to 210 °C, no obvious morphological changes were observed. However, when the reaction temperature was decreased from 150 to 120 °C, it was clearly seen from SEM images that the average diameter of TiO_2 spheres in the composites was found to increase from ca. 200 to 400 nm. The corresponding TEM results revealed that the TiO_2 sphere was transformed from single crystal (Figure 4d) to polycrystalline[39] (see SAED pattern recorded from the red circled area in Figure 5b), indicating that the crystal structure could be controlled by the hydrothermal reaction temperature. Figure 6 displays the SEM images of composites prepared under different reaction times. Apparently, all samples composed of MWCNTs and TiO_2 spheres with the average diameter of about 200 nm. It could be concluded that hydrothermal time exhibited negligible effect to the morphology of the composite photocatalysts, meaning hydrothermal time of 24 h was enough for the formation of these composite photocatalysts.

3.5. Adsorption and Photocatalytic Degradation of Gaseous Styrene. Herein, gaseous styrene was selected as a model organic pollutant to evaluate the photocatalytic activity of the MWCNTs-TiO_2 sphere composite photocatalysts. Figure 7 shows the adsorption, direct photolysis and photocatalytic

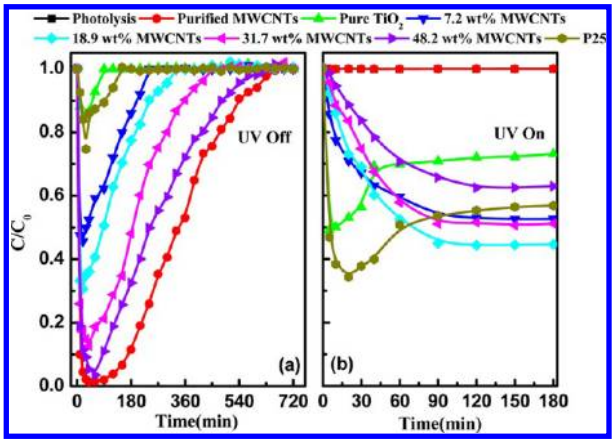

Figure 7. Adsorption, photolysis, and photocatalytic degradation kinetic curves of styrene by purified MWCNTs, pure TiO_2, P25, and the composite photocatalysts prepared with different contents of MWCNTs (TiO_2 contents, from 92.8 to 51.8 wt %; hydrothermal temperature, 150 °C; hydrothermal time, 72 h) .

degradation curves of styrene by purified MWCNTs, as-prepared pure TiO_2, Degussa P25, and as-prepared MWCNT–TiO_2 sphere composite photocatalysts with the different MWCNTs contents.

Before the lamp was switched on (Figure 7a), the adsorption equilibrium experiments were first conducted and the results showed that styrene was adsorbed swiftly on the samples at initial 20 min before slow breakthrough occurs (breakthrough point was observed where the outlet concentration of styrene was equal to 5% of the inlet concentration of styrene, indicating the beginning of the breakthrough[49]). For the as-prepared pure TiO_2 and P25, the complete breakthroughs (when the outlet and inlet concentrations of styrene were equal) were observed only after 90 and 150 min of adsorption, suggesting the poor adsorption capability of pure TiO_2 and P25 to styrene. However, for the adsorption of styrene on the composite sample prepared with the content of 7.2 wt % of MWCNTs,

dx.doi.org/10.1021/am3016476 | ACS Appl. Mater. Interfaces 2012, 4, 5988–5996

the time for complete breakthrough was apparently extended to 240 min. Moreover, when the composites contain 18.9, 31.7, and 48.2 wt % MWCNTs, the time for complete breakthrough were obtained as 330, 450, and 660 min, respectively. This means that the composite photocatalysts with higher MWCNTs content required longer time to reach the adsorption equilibrium, suggesting that MWCNTs played a key role in the adsorption of gaseous styrene. These results indicated that the time required for complete breakthrough followed an order of pure TiO_2 < P25 < MWCNT−TiO_2 sphere composite photocatalysts < purified MWCNTs, which was consistent with the order of BET surface area and BJH total pore volume. Clearly, purified MWCNTs exhibited the best adsorption capability that the complete breakthrough was achieved within almost 720 min because of large surface area and big pore volume of MWCNTs. All these results proved that the sample with larger surface area and bigger total pore volume possessed higher adsorption capacity to VOCs.

When the adsorption reached equilibrium, the lamp was switched on (Figure 7b). First, the control experiments of direct photolysis and photocatalytic degradation by purified MWNCTs were carried out and the results showed that more than 99% of styrene was left after 180 min of degradation, indicating only photolysis or purified MWCNTs could not efficiently decompose the styrene. The pure TiO_2 exhibited unstable and poor degradation activity to styrene. It could be seen from Figure 7b that a swift removal of styrene by pure TiO_2 could be discerned at first 10 min and higher than 50% of degradation efficiency was obtained. However, when the UV illumination went on for another 50 min, the degradation efficiency sharply decreased to 30.7% which continuously decreased to 26.9% within 180 min. Correspondingly, the color of the pure TiO_2 powder turned from white to yellow, which could be ascribed to the blockage of photocatalytic active sites by stable intermediates on the surface of TiO_2 during the photocatalytic reaction, thereby leading to the deactivation of the photocatalyst.[31,50−52] A similar result was obtained for the degradation of styrene by P25. A 43.2% of styrene was initially removed but degradation efficiency decreased with increased reaction time. In contrast, MWCNTs-TiO_2 sphere composite photocatalysts displayed more stable and higher styrene removal capability. With 7.2 wt % MWCNTs, the degradation efficiency stably increased at the first 90 min and slowly reached equilibrium within 120 min. The obtained steady-state degradation efficiency was 1.76 times of the pure TiO_2 and 47.3% of styrene can be removed within 180 min. An increase in the MWCNTs content to 18.9 wt % led to a degradation efficiency increase to 55.4%. Such dramatically enhanced photocatalytic efficiencies can be largely attributed to the synergetic effect of CNTs. In this work, the synergetic roles of CNTs in composite photocatalysts could be attributed to the improved electron pathway,[30,33] inhibited charge recombination,[30,33] and enhanced adsorption capability.[32] It could also attributed to the effect of CNTs as a structure regulator (i.e., acting as a dispersing template or support[31]) to affect the size of anatase TiO_2 spheres in the composites. Similar synergistic effect was also observed by Bouazza and co-workers[32] in the photocatalytic degradation of gaseous propene. However, when the MWCNTs contents was increased to 31.7 wt % or beyond (i.e., 48.2 wt %), instead of a positive synergetic effect, the degradation efficiency was slightly decreased to 48.8% and then sharply decreased to 37.1%. This could be ascribed to the light shielding effect of high content of MWCNTs.[33]

The above synergetic effect could also be affected by the effect of MWCNTs on the structural and physiochemical properties of the resultant composites. With the MWCNTs contents up to 18.9 wt %, the resultant TiO_2 spheres was still dominated and with exposed square-shaped {001} faceted surface. Under such circumstances, smaller particle size, larger BET surface area and bigger BJH total pore volume (Tables 1 and 2) are the positive attributes to the improved degradation efficiency. With high MWCNTs contents (i.e., 31.7 and 48.2 wt %), the decreased degradation efficiency could be attributed to the diminished {001} faceted surface and dramatically increased shielding effect[53] that overweighed other benefits of CNTs.

With the optimal 18.9 wt % MWCNTs content, the effects of the TiO_2 content, hydrothermal reaction temperature and time on the photocatalytic degradation of styrene were investigated (Figure 8). Figure 8a shows the degradation efficiency of

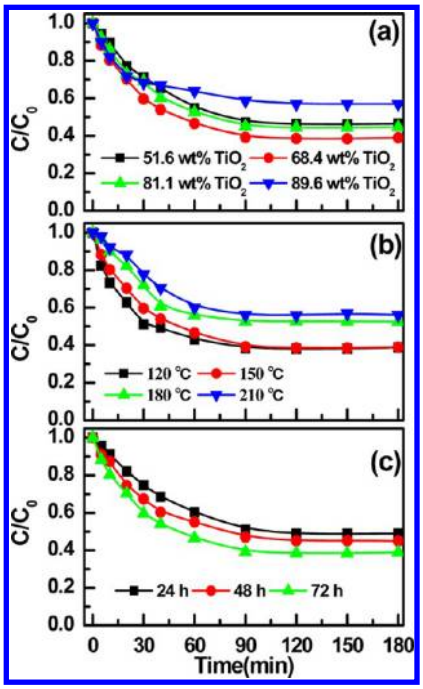

Figure 8. Photocatalytic degradation kinetic curves of styrene by the composite photocatalysts prepared (a) with different contents of TiO_2 (MWCNTs contents: from 48.4 to 10.4 wt %; hydrothermal temperature, 150 °C; hydrothermal time, 72 h); (b) under different hydrothermal temperatures (MWCNT content, 31.6 wt %; TiO_2 content, 68.4 wt %; hydrothermal time, 72 h); (c) under different hydrothermal times (MWCNTs content, 31.6 wt %; TiO_2 content, 68.4 wt %; hydrothermal temperature, 150 °C).

composite photocatalysts with different TiO_2 contents that followed the order of 89.6 wt % (43.0%) < 51.6 wt % (53.5%) < 81.1 wt % (55.4%) < 68.4 wt % (61.1%). The results indicated that the photocatalytic performance were largely dependent on the crystallite size[31] and dominant facets of TiO_2. For example, when the TiO_2 content was increased from 68.4 wt % to 81.1 wt %, the average size of TiO_2 particles increased from 26.7 to 30.1 nm, while the dominant {001} faceted TiO_2 spheres' surface was converted into {101} faceted surface (Figures 3d and 4d), which resulted in a decreased degradation efficiency from 61.1 to 55.4%. Figure 8b shows that an increase in the reaction temperature resulted in a decrease in the degradation efficiency, especially when the temperature was higher than 180 °C. These could be attributed mainly to the increased TiO_2

dx.doi.org/10.1021/am3016476 | ACS Appl. Mater. Interfaces 2012, 4, 5988−5996

particle size (Table 1) under high hydrothermal reaction temperatures. Figure 8c shows the effect of hydrothermal reaction time on the photocatalytic degradation performance toward styrene. It was found that an increase in the reaction time resulted in an increase in the degradation efficiency (i.e., from 51.1 to 55.0 to 61.1%), which could be attributed to increased synergistic interaction between TiO_2 and MWCNTs.

3.6. Photocatalytic Decolorization of MO in Water. To further demonstrate the synergistic effect in aqueous photocatalysis, we conducted the photocatalytic decolorization of MO, a well-known organic dye pollutant in wastewater produced from textile and other industrial processes[31] (see Figure S4 in the Supporting Information). It was found that with photolysis, purified MWCNTs, and pure TiO_2, only 5.6, 2.4, and 8.6% of MO decolorization efficiencies were achieved. In contrast, with 7.2 wt % MWCNTs, a remarkable increase indecolorization efficiency of 84.9% was obtained (see Figure S4a in the Supporting Information). With a further increase in the MWCNT content from 7.2 to 48.2 wt %, it was found that the decolorization efficiency followed an order of 48.2 wt % (72.8%) < 7.2 wt % (84.9%) < 31.7 wt % (86.9%) < 18.9 wt % (91.6%). Among them, 18.9 wt % MWCNTs showed the best photocatalytic performance toward the MO decolorization, which was the same as for the case of gaseous phase photocatalytic degradation of styrene. These results confirmed the existence of similar synergetic effects in aqueous phase photocatalysis. Figure S4b, c (Supporting Information) shows the effect of TiO_2 content and the reaction temperature on the MO decolorization performance. Almost identical trends as for the case of gaseous phase photocatalytic degradation of styrene were obtained. This further confirmed the existence of similar synergetic effects in aqueous phase photocatalysis.

4. CONCLUSIONS

In this work, a series of MWCNT−sub-micrometer-sized anatase TiO_2 sphere composite photocatalysts have been synthesized by a facial one-step hydrothermal method. The characterization results have confirmed that the important attributes affecting the photocatalytic performance including structural, dimensional, compositional, crystal facet, and physiochemical properties of the resultant composites can be significantly influenced by the presence of MWCNTs. Importantly, the photocatalytic degradation experimental results have demonstrated that such composite photocatalysts possess similar synergetic effects in both gaseous (i.e., styrene) and aqueous (i.e., MO) phase photocatalysis.

■ ASSOCIATED CONTENT

Ⓢ Supporting Information

Detailed experimental section and Figures S1−S4. This material is available free of charge via the Internet at http://pubs.acs.org.

■ AUTHOR INFORMATION

Corresponding Author

*Tel: +86-20-85291501 (T.A.); +61-7-555 2 8261 (H.Z.). Fax: +86-20-85290706 (T.A.); +61-7-5552 8067 (H.Z.). E-mail: antc99@gig.ac.cn (T.A.); h.zhao@griffith.edu.au (H.Z.).

Notes

The authors declare no competing financial interest.

■ ACKNOWLEDGMENTS

This is contribution IS−1519 from GIGCAS. This work was partially supported by the Team Project of Natural Science Foundation of Guangdong Province, China (S2012030006604), National Nature Science Foundation of China (21077104 and 40572173), Science and Technology Project of Guangdong Province, China (2009A030902003, 2011A030700003 and 2009B091300023), and the Cooperation Projects of Chinese Academy of Science with local government (ZNGZ-2011-005 and ZNGZ-2012-002).

■ REFERENCES

(1) Kim, M. S.; Liu, G.; Cho, H. K.; Kim, B. W. *J. Hazard. Mater.* **2011**, *190*, 537−543.
(2) Rene, E. R.; Montes, M.; Veiga, M. C.; Kennes, C. *Bioresour. Technol.* **2011**, *102*, 6791−6800.
(3) Prieto-Castello, M. J.; Amoros, D. M.; Garcia-Sagredo, J. M.; Llorens, A. C. *Toxicol. Lett.* **2011**, *205*, S64−S64.
(4) Teixeira, J. P.; Gaspar, J.; Coelho, P.; Costa, C.; Pinho-Silva, S.; Costa, S.; Da Silva, S.; Laffon, B.; Pasaro, E.; Rueff, J.; Farmer, P. *Mutagenesis* **2010**, *25*, 617−621.
(5) LeBot, M.; Bouzaza, A.; Martin, G.; Venot, S. *Environ. Technol.* **1996**, *17*, 819−829.
(6) Lim, M.; Zhou, Y.; Wood, B.; Wang, L. Z.; Rudolph, V.; Lu, G. Q. *Environ. Sci. Technol.* **2009**, *43*, 538−543.
(7) Lu, C. Y.; Lin, M. R.; Lin, J. C. *J. Hazard. Mater.* **2001**, *82*, 233−245.
(8) Georgieva, J.; Sotiropoulos, S.; Armyanov, S.; Poulios, I. *Int. J. Nanopart* **2011**, *4*, 216−230.
(9) Hager, S.; Bauer, R.; Kudielka, G. *Chemosphere* **2000**, *41*, 1219−1225.
(10) Fox, M. A.; Dulay, M. T. *Chem. Rev.* **1993**, *93*, 341−357.
(11) Hoffmann, M. R.; Martin, S. T.; Choi, W. Y.; Bahnemann, D. W. *Chem. Rev.* **1995**, *95*, 69−96.
(12) Liang, Y. Y.; Wang, H. L.; Casalongue, H. S.; Chen, Z.; Dai, H. J. *Nano Res* **2010**, *3*, 701−705.
(13) Zheng, Y.; Liu, J.; Liang, J.; Jaroniec, M.; Qiao, S. Z. *Energy Environ. Sci* **2012**, *5*, 6717−6731.
(14) Demeestere, K.; Dewulf, J.; Van Langenhove, H. *Crit. Rev. Environ. Sci. Technol.* **2007**, *37*, 489−538.
(15) Luo, H. Y.; Nie, X.; Li, G. Y.; Liu, J. K.; An, T. C. *Chinese J. Catal* **2011**, *32*, 1349−1356.
(16) An, T. C.; Zhang, M. L.; Wang, X. M.; Sheng, G. Y.; Fu, J. M. *J. Chem. Technol. Biotechnol.* **2005**, *80*, 251−258.
(17) Zhang, M. L.; An, T. C.; Fu, J. M.; Sheng, G. Y.; Wang, X. M.; Hu, X. H.; Ding, X. J. *Chemosphere* **2006**, *64*, 423−431.
(18) Chen, J. Y.; Li, G. Y.; He, Z. G.; An, T. C. *J. Hazard. Mater.* **2011**, *190*, 416−423.
(19) Zhang, M. L.; An, T. C.; Hu, X. H.; Wang, C.; Sheng, G. Y.; Fu, J. M. *Appl. Catal. A* **2004**, *260*, 215−222.
(20) Ma, C. Y.; Mu, Z.; Li, J. J.; Jin, Y. G.; Cheng, J.; Lu, G. Q.; Hao, Z. P.; Qiao, S. Z. *J. Am. Chem. Soc.* **2010**, *132*, 2608−2613.
(21) Liu, J. K.; An, T. C.; Li, G. Y.; Bao, N. Z.; Sheng, G. Y.; Fu, J. M. *Microporous Mesoporous Mater.* **2009**, *124*, 197−203.
(22) Sun, L.; An, T. C.; Wan, S. G.; Li, G. Y.; Bao, N. Z.; Hu, X. H.; Fu, J. M.; Sheng, G. Y. *Sep. Purif. Technol.* **2009**, *68*, 83−89.
(23) Wen, C. Z.; Jiang, H. B.; Qiao, S. Z.; Yang, H. G.; Lu, G. Q. *J. Mater. Chem.* **2011**, *21*, 7052−7061.
(24) Chen, J. S.; Chen, C. P.; Liu, J.; Xu, R.; Qiao, S. Z.; Lou, X. W. *Chem. Commun.* **2011**, *47*, 2631−2633.
(25) Matos, J.; Laine, J.; Herrmann, J. M. *Carbon* **1999**, *37*, 1870−1872.
(26) Matos, J.; Laine, J.; Herrmann, J. M. *Appl. Catal. B* **1998**, *18*, 281−291.
(27) Chen, J. Y.; Liu, X. L.; Li, G. Y.; Nie, X.; An, T. C.; Zhang, S. Q.; Zhao, H. J. *Catal. Today* **2011**, *164*, 364−369.
(28) Iijima, S. *Nature* **1991**, *354*, 56−58.

(29) Li, Z.; Gao, B.; Chen, G. Z.; Mokaya, R.; Sotiropoulos, S.; Puma, G. L. *Appl. Catal. B* **2011**, *110*, 50−57.
(30) Yu, J. G.; Ma, T. T.; Liu, S. W. *Phys. Chem. Chem. Phys.* **2011**, *13*, 3491−3501.
(31) Xu, Y. J.; Zhuang, Y. B.; Fu, X. Z. *J. Phys. Chem. C* **2010**, *114*, 2669−2676.
(32) Bouazza, N.; Ouzzine, M.; Lillo-Rodenas, M. A.; Eder, D.; Linares-Solano, A. *Appl. Catal. B* **2009**, *92*, 377−383.
(33) Yu, Y.; Yu, J. C.; Yu, J. G.; Kwok, Y. C.; Che, Y. K.; Zhao, J. C.; Ding, L.; Ge, W. K.; Wong, P. K. *Appl. Catal. A* **2005**, *289*, 186−196.
(34) Amano, F.; Prieto-Mahaney, O. O.; Terada, Y.; Yasumoto, T.; Shibayama, T.; Ohtani, B. *Chem. Mater.* **2009**, *21*, 2601−2603.
(35) Wang, Z. Y.; Lv, K. L.; Wang, G. H.; Deng, K. J.; Tang, D. G. *Appl. Catal. B* **2010**, *100*, 378−385.
(36) Nag, M.; Guin, D.; Basak, P.; Manorama, S. V. *Mater. Res. Bull.* **2008**, *43*, 3270−3285.
(37) Yang, H. G.; Sun, C. H.; Qiao, S. Z.; Zou, J.; Liu, G.; Smith, S. C.; Cheng, H. M.; Lu, G. Q. *Nature* **2008**, *453*, 638−641.
(38) Zhang, D. Q.; Li, G. S.; Yang, X. F.; Yu, J. C. *Chem. Commun.* **2009**, 4381−4383.
(39) Zhang, H. M.; Liu, P. R.; Li, F.; Liu, H. W.; Wang, Y.; Zhang, S. Q.; Guo, M. X.; Cheng, H. M.; Zhao, H. J. *Chem.—Eur. J* **2011**, *17*, 5949−5957.
(40) Wang, Y.; Zhang, H. M.; Han, Y. H.; Liu, P. R.; Yao, X. D.; Zhao, H. J. *Chem. Commun.* **2011**, *47*, 2829−2831.
(41) Yan, X. B.; Tay, B. K.; Yang, Y. *J. Phys. Chem. B* **2006**, *110*, 25844−25849.
(42) Xia, X. H.; Jia, Z. H.; Yu, Y.; Liang, Y.; Wang, Z.; Ma, L. L. *Carbon* **2007**, *45*, 717−721.
(43) Gao, B.; Chen, G. Z.; Puma, G. L. *Appl. Catal. B* **2009**, *89*, 503−509.
(44) Liu, G.; Wang, L. Z.; Yang, H. G.; Cheng, H. M.; Lu, G. Q. *J. Mater. Chem.* **2010**, *20*, 831−843.
(45) Kruk, M.; Jaroniec, M. *Chem. Mater.* **2001**, *13*, 3169−3183.
(46) Han, X. G.; Kuang, Q.; Jin, M. S.; Xie, Z. X.; Zheng, L. S. *J. Am. Chem. Soc.* **2009**, *131*, 3152−3153.
(47) Yang, H. G.; Liu, G.; Qiao, S. Z.; Sun, C. H.; Jin, Y. G.; Smith, S. C.; Zou, J.; Cheng, H. M.; Lu, G. Q. *J. Am. Chem. Soc.* **2009**, *131*, 4078−4083.
(48) Zhou, J. K.; Lv, L.; Yu, J. Q.; Li, H. L.; Guo, P. Z.; Sun, H.; Zhao, X. S. *J. Phys. Chem. C* **2008**, *112*, 5316−5321.
(49) Long, C.; Li, Y.; Yu, W. H.; Li, A. M. *J. Hazard. Mater.* **2012**, *203*, 251−256.
(50) Einaga, H.; Futamura, S.; Ibusuki, T. *Environ. Sci. Technol.* **2001**, *35*, 1880−1884.
(51) Mendez-Roman, R.; Cardona-Martinez, N. *Catal. Today* **1998**, *40*, 353−365.
(52) Peral, J.; Ollis, D. F. *J. Catal.* **1992**, *136*, 554−565.
(53) Zhang, H. M.; Han, Y. H.; Liu, X. L.; Liu, P. R.; Yu, H.; Zhang, S. Q.; Yao, X. D.; Zhao, H. J. *Chem. Commun.* **2010**, *46*, 8395−8397.